the FEBS Journal

Structural insights into bacterial resistance to cerulenin

Felipe Trajtenberg[1,*], Silvia Altabe[2,*], Nicole Larrieux[1], Florencia Ficarra[2], Diego de Mendoza[2], Alejandro Buschiazzo[1,3] and Gustavo E. Schujman[2]

1 Institut Pasteur de Montevideo, Unit of Protein Crystallography, Montevideo, Uruguay
2 Instituto de Biología Molecular y Celular de Rosario (IBR) – CONICET, Facultad de Cs Bioquímicas y Farmacéuticas, Universidad Nacional de Rosario, Argentina
3 Département de Biologie Structurale et Chimie, Institut Pasteur, Paris, France

Keywords
antibiotic resistance; bacteria; enzyme inhibitors; fatty acids; thiolase superfamily

Correspondence
G. E. Schujman, Instituto de Biología Molecular y Celular de Rosario (IBR) – CONICET, Facultad de Cs Bioquímicas y Farmacéuticas, Universidad Nacional de Rosario, Ocampo y Esmeralda, Predio CONICET Rosario, Rosario (S2000EZO), Argentina
Fax: +54 341 4237070 ext 607
Tel: +54 341 4237070
E-mail: schujman@ibr-conicet.gov.ar

*These authors contributed equally to this work.

(Received 17 January 2014, revised 10 March 2014, accepted 13 March 2014)

doi:10.1111/febs.12785

Cerulenin is a fungal toxin that inhibits both eukaryotic and prokaryotic ketoacyl-acyl carrier protein synthases or condensing enzymes. It has been used experimentally to treat cancer and obesity, and is a potent inhibitor of bacterial growth. Understanding the molecular mechanisms of resistance to cerulenin and similar compounds is thus highly relevant for human health. We have previously described a *Bacillus subtilis* cerulenin-resistant strain, expressing a point-mutated condensing enzyme FabF (FabF[I108F]) (i.e. FabF with isoleucine 108 substituted by phenylalanine). We now report the crystal structures of wild-type FabF from *B. subtilis*, both alone and in complex with cerulenin, as well as of the FabF[I108F] mutant protein. The three-dimensional structure of FabF[I108F] constitutes the first atomic model of a condensing enzyme that remains active in the presence of the inhibitor. Soaking the mycotoxin into preformed wild-type FabF crystals allowed for noncovalent binding into its specific pocket within the FabF core. Interestingly, only co-crystallization experiments allowed us to trap the covalent complex. Our structure shows that the covalent bond between Cys163 and cerulenin, in contrast to that previously proposed, implicates carbon C3 of the inhibitor. The similarities between *Escherichia coli* and *B. subtilis* FabF structures did not explain the reported inability of ecFabF[I108F] (i.e. FabF from *Escherichia coli* with isoleucine 108 substituted by phenylalanine) to elongate medium and long-chain acyl-ACPs. We now demonstrate that the *E. coli* modified enzyme efficiently catalyzes the synthesis of medium and long-chain ketoacyl-ACPs. We also characterized another cerulenin-insensitive form of FabF, conferring a different phenotype in *B. subtilis*. The structural, biochemical and physiological data presented, shed light on the mechanisms of FabF catalysis and resistance to cerulenin.

Database
Crystallographic data (including atomic coordinates and structure factors) have been deposited in the Protein Data Bank under accession codes 4LS5, 4LS6, 4LS7 and 4LS8.

Abbreviations
3D, three-dimensional; AAS, acyl ACP synthase; ACP, acyl carrier protein; bsFabF, FabF from *Bacillussubtilis*; ecFabF, FabF from *Escherichiacoli*; Fab[I108M], FabF with isoleucine 108 substituted by methionine; FabF[I108F], FabF with isoleucine 108 substituted by phenylalanine; FASI, type I fatty-acid synthase; FASII, type II or dissociated fatty-acid synthase; IPTG, isopropyl thio-β-D-galactoside; MIC, minimum inhibitory concentration; PDB, Protein Data Bank; TLS, translation libration screw; UFA, unsaturated fatty acid; wtFabF, wild-type FabF.

Introduction

Fatty acids are synthesized in all organisms via a repetitive cycle of four reactions, involving condensation, reduction and dehydration of carbon–carbon bonds. In higher organisms such as insects or mammals, these reactions are catalyzed on a type I fatty-acid synthase (FASI). In this large multifunctional protein, the growing fatty acid chain is covalently attached to the protein [1]. By contrast, in most bacteria, chloroplasts, mitochondria and apicoplasts, a type II or dissociated fatty-acid synthase (FASII) is used for *novo* fatty acid synthesis. This system employs a series of monofunctional proteins, each one catalyzing one step in the biosynthetic pathway, and reaction intermediates are carried through the cytosol as a thioester of the small acyl carrier protein (ACP) [2]. In fatty acid biosynthesis, the chain elongation step consists of the condensation of acyl groups, which are derived from acyl-ACP or acyl-CoA with malonyl-ACP. This reaction is catalyzed by the β-ketoacyl-ACP synthases, often referred as condensing enzymes [2]. These enzymes are classified into two groups. The first class of condensing enzymes (FabH type) is responsible for the initiation of fatty acid elongation and utilizes acyl-CoA primers [2]. *Escherichia coli* FabH selectively uses acetyl-CoA to initiate the pathway and fatty acids produced are of straight chain and unsaturated [2]. By contrast, *Bacillus subtilis* contains two FabH isozymes (FabHA and FabHB) that are selective for branched chain acyl-CoAs and produces mainly branched chain fatty acids [3]. Subsequent rounds of fatty acid elongation is carried out by the second class of condensing enzymes (FabB/FabF), which condense malonyl-ACP with acyl-ACP to extend the acyl chain by two carbons [2]. *E. coli* expresses both FabB and FabF condensing enzymes, whereas, in *B. subtilis*, only FabF carries out the successive elongation reactions in fatty acid synthesis [4,5]. Inhibition of this central reaction within the fatty acid synthesis pathway has been extensively studied towards the development of therapeutic applications in obesity, diabetes [6], cancer [7] and bacterial infections [8]. Several compounds have been isolated, specifically blocking the bacterial reaction, resulting in antibiotic compounds such as thiolactomycin [9], platensimycin [10] and platencin [11]. Cerulenin was the first FabB/FabF inhibitor to be identified. The condensing enzyme catalyzes the opening of the epoxide ring of cerulenin and the covalent modification of the active site cysteine [12]. Cerulenin has a 12-carbon acyl chain that associates with the hydrophobic channel accommodating the hydrocarbon chain of the acyl enzyme intermediate [13,14].

In the model Gram-positive organism *B. subtilis*, resistance to cerulenin is given by the *fabF1* allele coding for the FabF[I108F] protein (i.e. FabF with isoleucine 108 substituted by phenylalanine) [4]. Isoleucine 108 lies in the hydrophobic acyl chain-binding pocket of the FabF condensing enzymes and rotates to accommodate the acyl chain of cerulenin [14]. The replacement of Ile108 by Phe introduces a residue in the hydrophobic channel that cannot rotate to allow the optimum interaction between FabF and cerulenin [15]. Indeed, in the ecFabF (i.e. FabF from *E. coli*) condensing enzyme, the substitution I108F resulted in an enzyme insensitive to cerulenin, although its activity was limited to shorter (six carbon acyl-ACP) substrates [15]. Although the biochemical properties of ecFabF [I108F] (i.e. FabF from *Escherichia coli* with isoleucine 108 substituted by phenylalanine) suggest that this cerulenin-resistant enzyme would be unable to elongate acyl-ACPs *in vivo*, this prediction has not yet been received direct experimental support. FabF is the only elongation condensing enzyme in *B. subtilis* and, in contrast to *E. coli*, the bsFabF[I108F] enzyme (i.e. FabF from *B. subtilis* with isoleucine 108 substituted by phenylalanine) was active with a 14 carbon acyl-ACP substrate [4]. Moreover, although the fatty acyl chains of membrane phospholipids of bsFabF[I108F] is biased towards shorter fatty acyl chain groups [16], the mutant does not have a growth phenotype (in addition of its resistance to the antibiotic). To understand the apparent different behaviour of *B. subtilis* and *E. coli* FabF[I108F] enzymes, we determined the three-dimensional (3D) structures of wild-type FabF (wtFabF) from *B. subtilis*, both alone and in complex with cerulenin, as well as of the cerulenin-resistant FabF[I108F] point mutant. These structures provide important mechanistic insights into the mode of action of cerulenin, and reveal no significant differences from the available *E. coli* FabF structures. We further demonstrate *in vitro* and *in vivo* that ecFabF[I108F] efficiently elongates medium and long chain acyl-ACPs. Finally, we characterize a *B. subtilis* strain containing the FabF[I108M] mutant enzyme (i.e. FabF with isoleucine 108 substituted by methionine). These data shed new light on the mechanisms of resistance to this widely used inhibitor of fatty acid biosynthesis.

Results

Crystal structures of *B. subtilis* wtFabF and FabF [I108F]

To understand the structural bases of cerulenin-resistance in the FabF[I108F] enzyme of *B. subtilis*, as well

as the differential properties that have been reported for the same mutation in *E. coli*, we decided to solve the 3D structures of the *B. subtilis* enzymes. Both wtFabF and the FabF[I108F] point-mutant crystallized in similar mother liquors resulting in isomorphous orthorhombic crystals, containing one dimer per asymmetric unit. The diffraction data allowed us to solve both crystal structures at high resolution: 1.8 Å for wtFabF and 1.55 Å for the cerulenin-resistant FabF [I108F] (Table 1). Furthermore, we solved the structure of wtFabF in complex with cerulenin, both covalently and noncovalently (Table 1). Molecular replacement using the *Staphylococcus aureus* orthologue [Protein Data Bank (PDB) code: 2GQD, unpublished], readily identified a solution, which was refined, initially using noncrystallographic symmetry restraints (later released in the final stages) and a simple translation libration screw (TLS) model throughout [17], with one TLS body per chain. Refined electron density maps were very clear (Fig. 1A), allowing the entire chains to be traced, with one dimer per asymmetric unit. Only the N-terminal fused histidine tags (which were not removed before crystallization) were not visible, as well as 12 side chains, which were thus not included in the final model.

Structural comparison of the FabF[I108F] dimer with respect to the wild-type, displayed an overall rmsd of 0.17 Å (with 821 residues superposed), thus revealing almost identical structures, except for the point mutation and a derived, very slight local rearrangement of immediately neighboring side chains. Overall, FabF from *B. subtilis* (Fig. 1B) is structurally very similar to several condensing enzymes [13,18–20], displaying highest similarity to the orthologues from *S. aureus* and *Listeria monocytogenes* (3O04, unpublished), with which the sequence identities are close to 70% and the rmsd values are below 1 Å. The general architecture of these proteins groups them within the thiolase-like fold [21,22]. Within the dimer, each protomer is thus constituted by the conserved two-lobe thiolase core, which displays five layers of secondary structure elements αβαβα. There are currently a vast number of 3D structures that correspond to orthologous enzymes, displaying 1–3 Å rmsd and < 60% identity, including in the top positions the ones from *E. coli* (1KAS) and *Synechocystis* sp. (1E5M). Lower, yet significant similarity, is also found with the acetyl-CoA acetyltransferase (1M1T and related models), 3-hydroxy-3-methylglutaryl-CoA synthase (1XPK and related) and polyketide synthases among this large thiolase-related group of enzymes.

The molecular bases of cerulenin-resistance are clearly revealed by comparing the structures of the cerulenin-sensitive wild-type form of FabF, with the resistant point-mutant FabF[I108F] (Fig. 2). The mutation at position 108, substituting the wild-type Ile for a bulkier and more rigid Phe residue, introduces a major constraint with respect to accommodating the cerulenin long aliphatic chain within its binding tunnel. The phenyl group of F108 is predicted to clash against the last three carbons of the antibiotic acyl chain, not only explaining the resistance of the I108F mutant, but also its tendency to synthesize fatty acids of shorter length [4]. For FabF[I108F] to catalyze longer acyl chain condensations, this phenylalanine should move, and/or the last portion of the acyl chains fit unfavorably, with a consequent energetic penalty.

Binding of cerulenin to FabF

Previous work has postulated that cerulenin irreversibly binds covalently through its epoxide carbon C2 to the *E. coli* condensing enzymes FabF [14] and FabB [13]. The reactive nucleophile in the enzyme catalytic site is the thiol group of a conserved Cys, corresponding to Cys163 in *B. subtilis*. The *E. coli* enzymes have

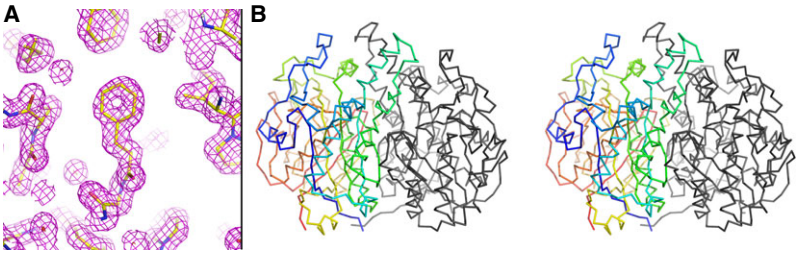

Fig. 1. Overall structure of FabF from *B. subtilis*, showing the final refined electron density maps and molecular model corresponding to the cerulenin-resistant I108F mutant of higher resolution. (A) Selected portion of the refined sigmaA-weighted ($2mF_o - DF_c$) Fourier electron density map, contoured at 1σ. (B) Ribbon cartoon of one FabF dimer as observed in the asymmetric unit. For clarity in distinguishing both monomers, one is colored in black, the other is colored in a blue to red ramp rainbow, highlighting the N- to C-terminal direction of the polypeptide chain. Note the pseudo-dyad axis relating one monomer to the other, from top to bottom in the plane of the paper.

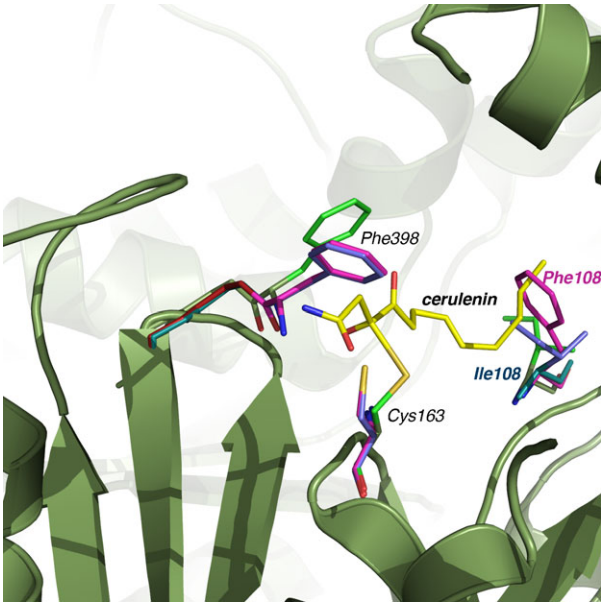

Fig. 2. Comparison between FabF wild-type, the I108F point-mutant and the wild-type covalently bound to cerulenin (intermediate state of the reaction). The cartoon representation shows a close up on the catalytic center of one of the monomers. For clarity, only selected side chains are shown. Side chain carbons colored blue correspond to the wild-type, colored magenta correspond to the I108F mutant, and colored green correspond to the wild-type in complex with cerulenin. Note the opening of F398 when cerulenin is bound within the acyl chain pocket. Note also the position of the benzene group of F108, expected to clash with the cerulenin chain.

been reported to be more sensitive to thiolactomycin inhibition than the *B. subtilis* homolog, confirming that subtle molecular differences among the condensing enzymes result in significant biological variations. In both cases, the antibiotic is indeed observed bound within the acyl-binding half of the reaction center (as opposed to the malonate side, outcompeted by inhibitor compounds such as thiolactomycin). As expected, the overall binding geometry is similar to those reported for the *E. coli* complexes (Fig. 3). In both complexes, the largest conformational rearrangements involve residues Phe398 (and the whole loop on which it resides), as well as Ile108, which move to make the extra space needed for the antibiotic to fit in the site snuggly. However, high resolution and clarity in the electron density maps allows us to add support for a few important observations that contrast with previously accepted hypotheses.

First, to trap the covalent intermediate, *B. subtilis* FabF appears to follow a transient conformational rearrangement that allows for the antibiotic to accommodate in its competent position to be attacked by the Cys163 SH group. This is supported by the fact that soaking experiments invariably resulted in noncovalent complexes, where cerulenin is observed as the epoxide tautomer, displaying a fairly flexible amide group (not as well defined in electron density as the rest of the compound). These results were obtained in five independent soaking experiments, revealing essentially identical crystal structures (data not shown). Co-crystallization in contrast, resulted in non-isomorphous crystals, although these were similar to the previous noncovalent complexes, which grow under a different crystallization condition. In this case, one cerulenin molecule is indeed bound covalently to the Cys163 of each monomer in the dimeric protein.

A second observation is also important in the context of previous findings: in the covalent complexes, the carbon atom on the cerulenin polar head that is bound to the thiol group of Cys163 is carbon C3 (Fig. 3B) and not C2 as has been postulated. Despite the clarity of the refined electron density maps, and to rule out any potential methodological artifact, we calculated omit maps excluding the antibiotic moieties from the model (Fig. 3B, inset) in accordance with a refinement protocol that includes simulated annealing to avoid model-derived phase bias. The covalent link is definitely observed between the sulfur atom of Cys163 and C3 of cerulenin, forming a thioether bond. It has been shown that free cerulenin is more stable in its hydroxylactam tautomer form in protic solvents [23,24], in equilibrium with an epoxide variant. From our noncovalent complexes, we are inclined to propose that the hydroxylactam form of cerulenin is not the main reactive species, probably as a result of the protein-defined hydrophobic environment of the binding tunnel.

ecFabF[I108F] elongates medium-chain acyl-ACPs

Structural comparison between FabF from *B. subtilis* (present study) and *E. coli* (PDB code: 1KAS) [18], unexpectedly reveals only minor differences, especially when analyzing the acyl-binding cavities. To ensure objective analyses apart from visual inspection and direct rmsd figures after superposition (0.93 Å rmsd, with 408 residues superimposed), variations were also assessed with ESCET [25] without revealing statistically significant differences. The differences identified are subtle and, in any case, comprise insufficient evidence to explain the alleged strong phenotypic difference between the *E. coli* and *B. subtilis* FabF enzymes, *vis-à-vis* cerulenin sensitivity. To shed light on this matter and to better understand cerulenin resistance, we re-characterized the biochemical properties of ecFabF

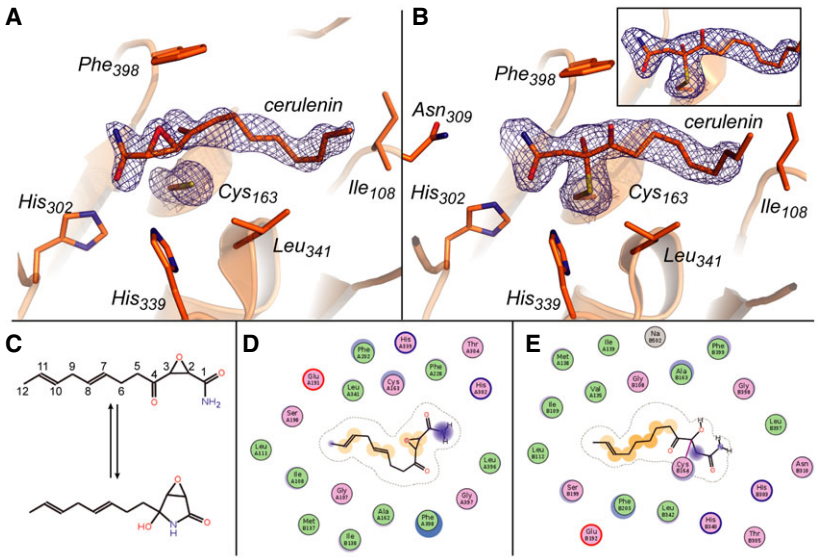

Fig. 3. Noncovalent versus covalent binding of cerulenin to *B. subtilis* FabF. (A) Electron density map (sigmaA-weighted $2mF_o - DF_c$ Fourier map, contoured at 1σ) corresponding to crystals of wtFabF soaked with cerulenin. C163 is the reactive cysteine; its thiol group was reproducibly found to be free, near the cerulenin epoxide ring. (B) Electron density map (sigmaA-weighted $2mF_o - DF_c$ Fourier, contoured at 1σ) corresponding to crystals of wtFabF co-crystalized with cerulenin (previously bound to the protein and the complex purified). Note the covalent connection between the thiol side chain of C163 and carbon C3 of cerulenin. Inset: simulated annealing omit map (sigmaA-weighted $2mF_o - DF_c$ contoured at 1σ), calculated with PHENIX (40), for the FabF:cerulenin complex, performed after excluding the two cerulenin molecules from the dimer model. The covalent bond involving cerulenin C3 is very clear. (C) Schematic representation of the epoxid (upper) and hydroxylactam (lower) tautomer structures of cerulenin, indicating the carbon numbering used (D, E) Two-dimensional diagram of the cerulenin in noncovalent (D) or covalent (E) complex with FabF, clarifying key interactions of the corresponding panels above (A and B). The view is rotated by approximately 180° according to a vertical axis in the plane of the paper, with respect to (A) and (B). Protein residues are labeled in circles, depicted as plain green for hydrophobic, pink for polar, pink with red line for acidic, and pink with blue line for basic residues. Images were prepared in COOT [39] and PYMOL [42].

[I108F]. Accordingly, two ORFs coding for either the predicted ecFabF or the mutant protein ecFabF [I108F] were expressed and purified as described in the Experimental procedures. The catalytic properties of ecFabF and ecFabF[I108F] were tested by performing enzyme assays based on the release of $^{14}CO_2$ from [3-^{14}C]malonyl-ACP when malonate is incorporated into acyl-ACPs. The resultant data (Table 3) show that the two enzymes readily accepted as substrates have short chain length 6:0-ACP and medium chain length 10:0-ACP, respectively. Although these data clearly demonstrate that ecFabF[I108F] is active with 10:0-ACP, they are not in agreement with results of a study by Val *et al.* [15] who reported that ecFabF [I108F] limited the substrate acceptance to 6:0-ACP. Because these experiments were performed using an enzymatic assay in which the incorporation of ^{14}C from [2-^{14}C]-malonate into a borohydride-reduced product is recorded, we used this technique to confirm that ecFabF[I108F] is active with 10:0-ACP. As expected, the kinetic constants for 10:0-ACP were essentially similar to those observed utilizing the decarboxylation method (data not shown). We also confirmed by both methods that ecFabF[I108F] remained insensitive to cerulenin 180 μM, whereas the wild-type enzyme activity dropped to 10% in presence of 90 μM antibiotic (data not shown). These results suggest that the mutation I108F in FabF of both *B. subtilis* and *E. coli* generates a cerulenin-resistant enzyme containing a fatty acid substrate-binding pocket with similar chain length specificity.

To confirm that ecFabF[I108F] is able to synthesize long chain fatty acids *in vivo*, we attempted to test the ability of $fabF_{Ec}$ and $fabF1_{Ec}$ to functionally replace the growth defect of a *fabF* conditional knockout strain of *B. subtilis*. However, we failed to functionally express $FabF_{Ec}$ in *B. subtilis* (data not shown), probably because $fabF_{Ec}$ contains several codons that are rarely used in *B. subtilis*. Because *B. subtilis* does not provide a suitable system for testing the function of $FabF1_{Ec}$, we resorted to the *E. coli* CY288 strain, which carries a *fabF* null mutation plus a temperature-sensitive $fabB^{ts}$ mutation. As expected from previous data, strain CY288 is nonviable at 42 °C because of

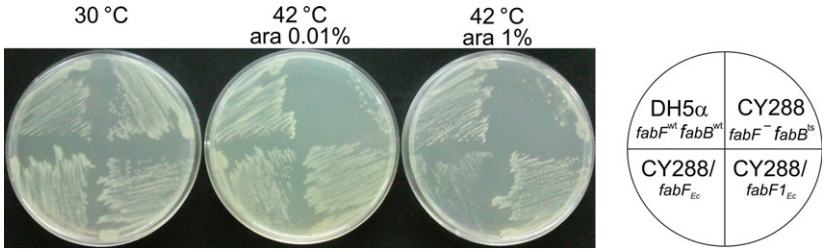

Fig. 4. *E. coli* FabF1 is functional *in vivo*. Strains DH5α (wt), CY288 (*fabF*$^{-}$ *fabB*^{ts}), GS581 (CY288 P_{BAD}-*fabF*$_{Ec}$) and GS582 (CY288 P_{BAD}-*fabF1*$_{Ec}$) were incubated for 24 h at the indicated temperatures on LB plates containing different amounts of the inducer arabinose.

the lack of FabB and FabF activities resulting in the failure of unsaturated fatty acid (UFA) supplementation to support growth (Fig. 4). The lack of growth of *fabF*$^{-}$ *fabB*^{ts} double mutant strain is a result of its inability to elongate any nascent fatty acyl chain produced by FabH to the chain lengths required for synthesis of essential membrane lipids [26]. Therefore, even in the presence of UFA supplementation, these strains fail to grow because they are unable to synthesize the saturated fatty acid chains required for phospholipids and the essential lipid A component of the outer membrane. Strain CY288 was transformed with plasmids pGES490 and pGES491 that encode, respectively, the *fabF1*$_{Ec}$ or the wild-type *fabF*$_{Ec}$ genes under the control of the P*xyl* promoter. As expected, the strain containing the empty vector pGES247 was nonviable at the nonpermissive growth temperature (42 °C) even in the presence of an exogenous UFA (data not shown). By contrast, cultures of CY288 containing either *fabF*$_{Ec}$ or *fabF1*$_{Ec}$ grew at 42 °C in the presence of an exogenous UFA. Similar results were obtained when strain CY288 was transformed with plasmid pGES554, which encoded *fabF1*$_{Ec}$ under the control of the P_{BAD} promoter present in the low copy number pBAD322 vector (Fig. 4). Using this expression system, functional complementation of CY288 was obtained with *fabF1*$_{Ec}$, even with very low concentrations of the arabinose inducer (i.e. 0.01% w/v) (Fig. 4). Thus, this experiment ruled out the possibility that $FabF1_{Ec}$ replaces wild-type $FabF_{Ec}$ only when the mutant protein is overexpressed. These results confirm that ecFabF[I108F] can catalyze the elongation of all the acyl-ACP intermediates required to synthesize the long-chain fatty acyl-ACPs needed for membrane phospholipids and lipid A.

Characterization of bsFabF[I108M]

Previous work reported that extracts of *B. subtilis* strain GS77, expressing the FabF[I108F] isoform, demonstrated FASII activity that was approximately seven-fold higher than extracts expressing wtFabF [4]. Further experiments indicated that most of the genes encoding for the FAS system were overexpressed in this strain, and this was necessary both for cerulenin resistance and normal cell growth [16]. The only phenotype associated with FabF[I108F] was its resistance to cerulenin. During these experiments, we isolated another *B. subtilis* strain resistant to cerulenin which was named GS76. This strain was four-fold more resistant to cerulenin [minimum inhibitory concentration (MIC) = 20 $\mu g \cdot mL^{-1}$] than the wild-type isogenic strain JH642 (MIC = 5 $\mu g \cdot mL^{-1}$) but less resistant than the GS77 strain (MIC = 40 $\mu g \cdot mL^{-1}$). To determine whether the mechanism responsible for cerulenin resistance of strain GS76 was related to a deficiency in the uptake or excess secretion of the antibiotic or whether it contained a FabF allele coding for an enzyme insensitive to the inhibitor, we obtained crude protein extracts from wild-type and mutant strains and assayed *in vitro* the FASII activities in the presence or in the absence of cerulenin. These experiments showed that the GS76 FASII activity was only slightly reduced by 10 $\mu g \cdot mL^{-1}$ of cerulenin, whereas the wild-type extract activity was markedly inhibited by the antibiotic (Table 4). This result indicates that GS76 synthesizes a FASII resistant to cerulenin instead of containing a mutation inhibiting the transport of the antibiotic or enhanced detoxification of cerulenin. The *fabF* allele from strain GS76 was amplified and sequenced, indicating that the ORF has a C→G transversion in position 327 from the translation start. In the protein sequence, this mutation results in the substitution of isoleucine 108 on the wild-type enzyme to a methionine in the mutant allele. Thus, we named this new *B. subtilis fabF* allele as *fabF3*. To confirm that this allele is responsible for cerulenin resistance, we constructed the diploid strain FF16 containing an isotopic copy of GS76 *fabF* and an ectopic copy of wild-type *fabF* under the control of P*spac* [inducible by isopropyl thio-β-D-galactoside (IPTG)] and P*xyl* (induced by xylose), respectively (Table 2). In the

Table 1. X-ray diffraction data processing and refinement statistics.

	wtFabF	FabF I108F mutant	wtFabF + cerulenin noncovalent complex	wtFabF + cerulenin covalent complex
Space group	$P2_12_12_1$	$P2_12_12_1$	$P2_12_12_1$	$P2_12_12_1$
Wavelength (Å)	1.5418	1.5418	1.5418	1.5418
Data resolution (Å)[a]	28.9–1.8 (1.9–1.8)	29.0–1.56 (1.64–1.56)	29.24 1.67 (1.76–1.67)	30–2.10 (2.21–2.10)
Measured reflectance	295 602	594 632	370 657	207 898
Multiplicity[a]	3.5 (3.3)	4.5 (3.4)	3.5 (3.4)	4.1 (4.1)
Completeness (%)[a]	99.8 (99.1)	100 (99.9)	98.9 (95.4)	97.4 (95.5)
R_{meas} (%)[a,b]	0.062 (0.656)	0.046 (0.367)	0.054 (0.521)	0.065 (0.490)
$<I/\sigma(I)>$[a]	13.4 (2.1)	19.1 (3.6)	16.8 (2.5)	14.1 (3.0)
Cell parameters *a*, *b*, *c* (Å)	72.5, 87.5, 144.6	72.1, 88.0, 145.0	72.3, 87.7, 144.7	86.4, 87.6, 116.4
Refinement resolution (Å)	27.9–1.8	22.8–1.56	28.9–1.67	29.1–2.10
R_{cryst} (number of refinements)[c]	16.2 (83 737)	14.9 (130 183)	15.1 (99 202)	16.2 (50 776)
R_{free} (number of refinements)[c]	19.5 (1616)	17.2 (1258)	18.0 (1945)	18.7 (792)
rmsd bond length (Å)	0.007	0.010	0.007	0.009
rmsd angle (°)	1.076	1.050	1.111	1.060
Protein nonhydrogen atoms	6992	6299	7147	6138
Water molecules	686	951	704	393
Ligand atoms	4 (K^+)/24 (GOL)	3 (K^+)/1 (Cl^-)/30 (GOL)	4 (K^+)/24 (GOL)/32 (CER)	3 (Na^+)/1 (Cl^-)/32 (CER)/12 (EDO)
PDB code	4LS5	4LS6	4LS7	4LS8

[a] Values in parentheses apply to the high-resolution shell. [b] $R_{meas} = \sum_h \sqrt{N_h/(N_h-1)} \sum |I_i - \langle I\pm\rangle| / \sum_h \sum_i I\pm$; N_h, multiplicity for each reflection; I_i, the intensity of the i_{th} observation of reflection h; $<I>$, the mean of the ^{i} intensity of all observations of reflection h, with $I\pm = 1/N_h \sum_i (I_{(-)} \text{or } I_{(+)})$; $\sum_h$ is taken over all observations of each reflection. [c] $R = \sum_h |F(h)\text{obs} - F(h)\text{calc}| / \sum_h |F(h)\text{obs}|$; R_{cryst} and R_{free} were calculated using the working and test *hkl* reflection sets, respectively. $\sum_h \sum_i$

absence of both inducers, strain FF16 failed to grow because no *fabF* gene is expressed. Xylose-induced expression of wild-type *fabF* allowed growth of FF16 but did not confer resistance to cerulenine (Table 5). However, in the presence of IPTG strain, FF16 was able to grow in the presence of 10 $\mu g \cdot mL^{-1}$ of the inhibitor (Table 5). These results confirm that GS76 synthesizes a FabF enzyme that is resistant to cerulenin inhibition.

Strikingly, two differences were observed between FabF[I108F], contained in GS77, and FabF[I108M], contained in GS76. GS77 was two-fold more resistant to cerulenin than GS76, and its FASII activity was seven-fold higher than that of the wild-type and GS76 strains. We have previously shown that the substitution I108F constrains the acyl acceptance to short acyl-ACPs resulting in the accumulation of malonyl-CoA [16]. The binding of malonyl-CoA to the global regulator of fatty acid biosynthesis FapR impairs the productive association of the protein to the *fap* operators, increasing the expression level of several genes that constitute the *fap* regulon in GS77 [16]. To test whether *fabF3* has the same effect as *fabF1* on the expression of the *fap* regulon, we used *B. subtilis* strains containing, either the *fabF*, *fabF1* or *fabF3* alleles, as well as a P*fabHAF-lacZ* transcriptional fusion at the non-essential *amyE* locus. The β-galactosidase activities of the different strains were then compared. As shown in Fig. 5, transcription of *fabHAF-lacZ* is upregulated only in the strain containing *fabF1*. It follows that only the *fabF1* allele caused the accumulation of malonyl-CoA and malonyl-ACP, indicating that the FabF [I108M] isoform appears to synthesize normal long chain fatty acids.

Discussion

The structural and functional characterization of FabF from *B. subtilis* that we report reveals the molecular basis for the resistance to cerulenin that arises by natural point mutations in this condensing enzyme. Phenylalanine represents a larger and more rigid side chain compared to wild-type isoleucine. Position 108 is a key location, in tight association with the growing acyl chain when it reaches a certain length, as well as determining the actual volume of the acyl-lodging cavity;

Table 2. Bacterial strains and plasmids.

Strain or plasmid	Relevant characteristics	Source/reference
Strains		
Bacillus subtilis		
JH642	*trpC2 pheA1*	Laboratory stock
GS77	JH642 *fabF1* (FabF[I108F])	Schujman *et al.* [48]
GS76	JH642 *fabF3* (FabF[I108M])	Present study
GS37	JH642 *amyE*::P*fabHAF-lacZ*:*cat*	Schujman *et al.* [4]
GS41	GS77 *amyE*::P*fabHAF-lacZ*:*cat*	Schujman *et al.* [4]
FF8	GS76 *amyE*::P*fabHAF-lacZ*:*cat*	Present study
FF13	JH642 *fabHAF*::pMutin4 (P*fabHAF–lacZ*, P*spac-fabHAF), thrC*::P*xylA-fabF1*	Present study
FF14	JH642 *fabHAF*::pMutin4 (P*fabHAF–lacZ*, P*spac-fabHAF), thrC*::P*xylA-fabF*	Present study
FF16	GS76 *fabHAF*::pMutin4 (P*fabHAF3–lacZ*, P*spac-fabHAF3), thrC*::P*xylA-fabF*	Present study
Escherichia coli		
DH5α	*supE44 thi-1 ΔlacU169(ϕ80lacZΔM15) endA1 recA1 hsdR17 gyrA96 relA1 trp6 cysT329::lac* $inm^{\lambda.pI(209)}$	Laboratory stock
M15[pREP4]	nal^S str^S rif^S thi^- lac^- ara^+ gal^+ mtl^- F^- $recA^+$ uvr^+ lon^+	Qiagen
BL21(DE3)	*F ompT gal dcm lon* $hsdS_B(r_B^- m_B^-)$ *λ(DE3 [lacI lacUV5-T7 gene 1 ind1 sam7 nin5])*	Laboratory stock
CY288	*fabF fabB(Ts)*	de Mendoza *et al.* [33]
GS484	M15[pREP4] $fabF_{Ec}{}^{I108F}$-his_6	Present study
GS581	CY288 P_{BAD}-$fabF_{Ec}$	Present study
GS582	CY288 P_{BAD}-$fabF1_{Ec}$	Present study
Plasmids		
pBAD322	*E. coli* cloning vector; contains arabinose inducible P_{BAD} promoter, Amp^r	Cronan [49]
pQE32	*E. coli* cloning vector; Amp^r	Promega
pGES204	pMutin4 + 5′$fabHA_{(from\ -58\ to\ +383\ of\ initial\ ATG)}$	Present study
pGES247	Integrates in *amyE*, contains xylose inducible P*xylA* promoter, $spec^R$	Albanesi *et al.* [32]
pGES478	pGES247 + $fabF_{Ec}{}^{wt}$	Present study
pGES479	pGES247 + $fabF_{Ec}{}^{I108F}$	Present study
pGES480	pQE32 + $fabF_{Ec}{}^{I108F}$	Present study
pGES553	pBAD322 + $fabF_{Ec}{}^{wt}$	Present study
pGES554	pBAD322 + $fabF_{Ec}{}^{I108F}$	Present study
pMSD8	Encode the four acetyl CoA carboxylase subunits, Amp^r	Davis *et al.* [50]

Table 3. Kinetic parameters of *E. coli* FabF and FabF[I108F][a].

Substrate	Parameter	$FabF_{Ec}$	$FabF[I108F]_{Ec}$
Hexanoyl-ACP	K_m (μM)	7.8 ± 1.2	7.8 ± 0.5
	V_{max} (pmol·μg^{-1}·min^{-1})	10.2 ± 1.2	30.4 ± 1.7
Decanoyl-ACP	K_m (μM)	11.0 ± 0.9	44.6 ± 0.5
	V_{max} (pmol·μg^{-1}·min^{-1})	51.0 ± 5.3	11.3 ± 1.1

[a]Reported values are from one measurement representative of four independent experiments.

Table 4. Effect of cerulenin (10 μg·mL^{-1}) on *in vitro* synthesis of fatty acids by cell free extracts.

	Specific activity[a] (pmol·min^{-1}·mg protein^{-1})	
Strain	− cerulenin	+ cerulenin
JH642	4.1	1.1 (28%)[b]
GS76	4.0	3.0 (75%)

[a] Activities were determined in cell extracts as described in the Experimental procedures. [b] Residual activity relative to the untreated cell extract.

hence, there is high sensitivity in the phenotypic results associated with particular mutations.

The size of the side chain at position 108 appears to be a major parameter correlated with cerulenin resistance. This can be clearly seen with the phenylalanine substitution, given that the Ile residue occupies approximately 170 Å^3, compared to the bulkier Phe side chain, which increases its volume to approximately 200 Å^3

Table 5. Growth of merodiploid *fabF* mutant strains in the presence of different inducers and cerulenin.

Strain	Genotype	Growth[a]				
		(–)	IPTG 0.5 mM	Xylose 0.5%	IPTG 0.5 mM, Cer 10 μg·mL^{-1}	Xylose 0.5%, Cer 10 μg·mL^{-1}
FF16	P*spac-fabF3*, P*xyl-fabF*	–	+	+	+	–
FF13	P*spac-fabF*, P*xyl-fabF1*	–	+	+	–	+
FF14	P*spac-fabF*, P*xyl-fabF*	–	+	+	–	–

[a] Strains were grown in LB plates at 37 °C for 24 h in the presence of inducers and/or cerulenin, as indicated.

[27]. This larger volume is predicted to cause direct steric hindrance, hampering enzyme function (FabF[I108F] accumulates malonyl-CoA and requires overexpression of FabF for proper growth) and also resulting in higher resistance to cerulenin (MIC = 5 μg·mL^{-1} versus 40 μg·mL^{-1} for wtFabF and FabF[I108F], respectively). An intermediate phenotype was seen with the I108M substitution (MIC = 20 μg·mL^{-1}), which, however, does not accumulate malonyl-CoA, thus behaving similar to the wild-type with respect to its ability to accommodate longer acyl chains. This is consistent with the fact that Ile and Met are almost isosteric, a much more subtle structural modification, whereby steric hindrance is not expected to affect longer acyl chains to grow within the cavity. However, the lower hydrophobicity of Met compared to Ile [28] may well be the basis of decreased cerulenin binding because, as noted above, position 108 is a key site establishing direct contact with the acyl chain.

A striking observation concerns the nature of the covalent bond between FabF and cerulenin, which we have observed to occur between the Cys163 thiol group and carbon C3 of the antibiotic. A direct nucleophilic attack of the thiol on carbon C3 should resolve with the opening of the epoxide, leaving the oxygen atom as a hydroxyl group on carbon C2. However, in our structure, we clearly see that the hydroxyl group is still bound to C3 (C2 is a methylene). To exclude a potential modeling error, we performed subsequent refinement cycles starting with our final model, although this was modified such that the hydroxyl group was forced to be bound to C2, with C3 remaining as a tertiary carbon. With or without simulated annealing, the results undoubtedly support our current model, with very strong difference Fourier peaks indicating the true position of the OH (Fig. 6). This strongly suggests a more complex mechanism of reaction: the thiol group may initially attack either carbon C2 or C3, so that the intermediate subsequently suffers a rearrangement, eventually shifting the OH from C2 to C3 or, instead, the Cys163 SH group might end up bonding to C3. It appears that under, unrestrained

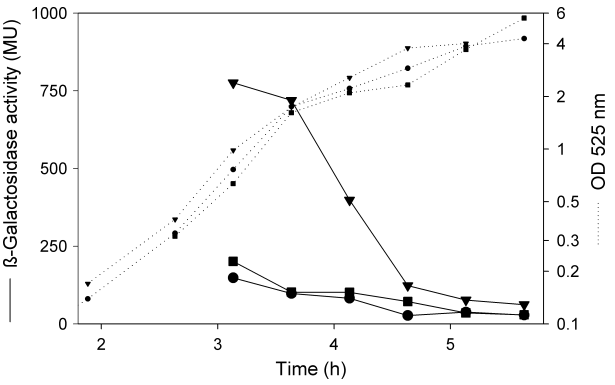

Fig. 5. Expression of the *fap* regulon in wild-type, *fabF1* and *fabF3* background. *B. subtilis* strains GS37 (wild-type, circles), GS41 (*fabF1*, triangles) and FF8 (*fabF3*, squares) harboring a P*fabHAF–lacZ* fusion located in the *amyE* locus were grown in LB medium at 37 °C. Growth was monitores by measuring culture absorbance at 525 nm (dotted lines). At the indicated times, samples of each culture were removed to assay β-galactosidase specific activity (solid lines). A single experiment representative of four repeats is shown.

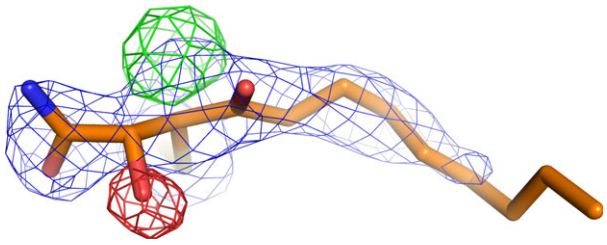

Fig. 6. Electron density map (sigmaA-weighted $2mF_o - DF_c$ Fourier map, contoured at 1.2σ, and sigmaA-weighted $mF_o - DF_c$ Fourier map, contoured at 3.5σ) corresponding to crystals of the covalent complex between *B. subtilis* wtFabF and cerulenin. The model used in this re-refinement was modified changing the position of the hydroxyl group from carbon C3 (as observed in the crystal structure reported, see main text) towards C2. Note the resulting positive difference Fourier peak on C3 (7.1σ), whereas a negative peak at the refined position on C2 is also observed (4.8σ). These results comprise strong evidence supporting a quaternary C3 carbon configuration, bound to both the OH group and the SG of Cys163.

conditions (i.e. working with free cysteine as a nucleophile), the reaction occurs by a direct nucleophilic attack to carbon C2 [24], with the epoxide oxygen migrating to C3, without further rearrangements. The fact that previous FabF [14] and FabB [13] crystallographic reports followed the initial hypotheses based on spontaneous cerulenin reactivity is probably derived from the lower quality of the electron density maps that could be analyzed. *E. coli* FabF crystals were fragile, resulting not only in limited resolution (2.65 Å), but also in rather incomplete diffraction data. In the case of the 2.27 Å resolution FabB structure, although the data are indeed better, the electron density is ambiguous with respect to defining the actual connection between the cerulenin moiety and the catalytic Cys. We reanalyzed these latter results from the PDB with further refinement [29] and it was strongly suggested that the bond is indeed made with cerulenin C3, with otherwise negative $F_o - F_c$ peaks on the modeled O1 (bound to C4) that can be satisfactorily corrected using our interpretation. Further studies need to be conducted to reveal the mechanistic details of the trans-acylation reaction within the protein catalytic site environment. In any case, the observed difference from previous reports implies a slight but measurable shift in the actual position of the covalent cerulenin residue, with potential implications for target-based drug-design.

The catalytic properties previously reported for the point mutation I108F for the FabF enzymes of *B. subtilis* or *E. coli* suggested that there should be structural differences between both proteins. However, the structural comparison did not reveal any relevant molecular differences that would explain these functional discrepancies when using long-chain acyl-ACPs as substrate. The acyl-binding cavities show very similar volumes, ranging between 35 and 50 $Å^3$, with the *E. coli* protein at the higher end of the range. The most significant differences lay instead on the malonate-binding half-site near the reaction center, where *B. subtilis* displays important substitutions on the N-terminal end of a helix that includes larger residues, Tyr307-Tyr308-Asn309 (Pro-Ala-Gly in *E. coli*). These bulkier side chains in the *B. subtilis* enzyme partially occlude the entrance of the binding-pocket. Although these modifications might affect binding and sensitivity to malonate-competing compounds (such as thiolactomycin or platencimycin), they do not appear to support potential cerulenin-binding modulation at the growing acyl half-site. Deep in the acyl-binding tunnel, minor differences can be identified, which could affect the fine-tuning of the acyl-chain length preference and/or antibiotic sensitivities. Specifically, the residues Ala192 and Pro193 in *B. subtilis*, correspond to Lys192 and Ala193, respectively, in *E. coli*. Pro193 is approaching residue 108 from the end of the acyl-binding tunnel. If wild-type Ile108 is changed to a phenylalanine, Pro193 comes into van der Waals contact (3.8 Å among the nearest Phe108-Pro194 carbon atoms). The substitution of this proline to an alanine in the *E. coli* enzyme might be able to modulate the ability of the enzyme to accommodate Phe108 movements. Overall, given their structural resemblance, we eventually hypothesized that both proteins should have the same catalytic properties. We therefore performed a detailed *in vitro* and *in vivo* characterization, confirming that both proteins are able to similarly use long-chain acyl-ACPs as substrate and that the same resistance mechanism is involved.

Taken together, our results highlight the importance of residue 108 of FabF both with respect to the length of acyl-ACPs that the enzyme is able to elongate, as well as its resistance to cerulenin. As the size and rigidity of the amino acid residue in that position increases, the enzyme becomes less efficient in the elongation of long-chain acyl-ACPs, consequently conferring higher levels of resistance to the antibiotic.

Experimental procedures

Construction of strains

Strains and relevant plasmids used in the present study are listed in Table 2. The *E. coli* malonyl-CoA:ACP transacylase (MCAT) gene cloned in the expression vector pET15b (Novagen, Madison, WI, USA) was kindly provided by Dr C. Rock, [30]. The *E. coli* β-ketoacyl-ACP synthase I (KAS I) gene cloned in the expression vector pQE30 (Qiagen, Calencia, CA, USA) was a much appreciated gift from Dr K. Dehesh [31].

To generate *E. coli fabF* coding for the mutation I108F, SOEing PCR was employed with primers fabFcolExpUp (5′-GAGTTTAAGCTTTTTGTCCCACTAGAATC-3′), fabFcolI108FRev (5′-GCCAAACCCGGAGCCAATTG-3′), fabFcolI108FFow (5′-GCAATTGGCTCCGGGTTTGG-3′) and fabFcolExpLow (5′-ATAACGGTGGATCCTGACAACTTAGATC-3′), using *E. coli* DNA as template. *E. coli fabF* gene was amplified from *E. coli* DNA using primers fabFcolExpUp and fabFcolExpLow. Both genes were cloned in pTOPO (Life Technologies, Grand Island, NY, USA), generating plasmids pGES475 ($fabF_{Ec}{}^{wt}$) and pGES476 ($fabF_{Ec}{}^{I108F}$); their sequences were verified and the genes were subcloned into pGES247 [32] to obtain plasmids pGES478 and pGES479, respectively, and into pBAD322 generating plasmids pGES553 ($fabF_{Ec}{}^{wt}$) and pGES554 ($fabF_{Ec}{}^{I108F}$). Transformation of strain CY288 [33] with plasmids

pGES553 and pGES554 generated strains GS581 and GS582, respectively. To clone $fabF_{Ec}^{I108F}$ in pQE32, the gene was re-amplified with primers fabFcolHis6Up (5′-CCTA GAGGATCCACTTGTCTAAGCGTCGTG-3′) and fabF-colHis6Low (5′-CTGTTATAAGCTTGGAAAATGACAA CTTAGATC-3′) using pGES476 as template. The resulting plasmid pGES480 was transformed into the expression strain M15 to obtain strain GS484.

To obtain strains FF13 and FF14, strain GS203 was transformed with plasmids pGES420 or pGES419 [16], respectively. Strain GS203 was obtained by transformation of wild-type strain JH642 with pGES204. pGES204 is derived from pMUTIN4 [34] and contains the first 481 bases of *fabHA*, PCR amplified from JH642 DNA using primers RegFow (5′-TACCTGAAGCTTATAATTGATC ACAACCTGA-3′) and yjaXSac2 (5′-TTGCCGCGGATT CAATAAATTGTTT-3′). Strain FF16 was obtained by transformation of strain GS76 with pGES204 and then with pGES419. Strain FF08 was obtained by transformation of strain GS76 with pGES35 [4].

Protein expression and purification

Acyl ACP synthase (AAS) from *Vibrio harveyi* B392 was expressed and purified from *E. coli* strain YFJ239 [35]. All *E. coli* strains were grown at 37 °C in LB medium supplemented with ampicillin and/or kanamycin. IPTG was used to a final concentration of 1 mM. Proteins were purified as detailed previously [30]. Protein concentrations were determined by the Lowry method. Aliquots were stored frozen and diluted to suitable concentrations with storage buffer before analysis. SDS/PAGE analysis was performed by the method of Laemmli.

For crystallization purposes, wtFabF and the mutant FabF[I108F] were purified by Ni^{2+}-affinity chromatography using a HisTrap column (GE Healthcare, Milwaukee, WI, USA) and then injected into a HiLoad 16/600 Superdex 200 prep grade column (GE Healthcare) pre-equilibrated with 20 mM Tris-HCl (pH 8), 150 mM NaCl, 1 mM EDTA and 0.5 mM dithiothreitol. After size exclusion chromatography, both proteins were concentrated to 12 $mg{\cdot}mL^{-1}$ by ultrafiltration (Vivaspin; GE Healthcare) and stored in aliquots at −80 °C for further use in crystallization trials.

Protein crystallization

Crystals of FabF[I108F] were grown using the vapor-diffusion method, mixing equal amounts of protein and reservoir solutions [12% poly(ethylene glycol) 3350, 0.2 M KCl] in drops of 4 μL. The first crystals appeared in < 24 h. wtFabF crystals grew under slightly different conditions [10% poly(ethylene glycol) 3350, 0.25 M KCl], using crystals of FabF[I108F] as a source of microseeds. Soaking cerulenin at 10 $mg{\cdot}mL^{-1}$ for 30 min on wtFabF crystals allowed us to obtain the structure of the noncovalent complex. The covalent complex was obtained by co-crystallization, preincubating the protein for 1 h in a 10 M excess of cerulenin. The protein–cerulenin complex was thereafter injected into a Superdex 200 10/300 GL column (GE Healthcare), concentrated at 12 $mg{\cdot}mL^{-1}$ and crystallization drops prepared as above but with a different reservoir solution [15% poly(ethylene glycol) 3000, 0.1 M sodium citrate, pH 5.5]. Single crystals appeared 1 week later. Crystals were cryoprotected in their respective mother liquors containing 25% glycerol, and flash frozen in liquid N_2.

Diffraction, data collection and structure determination

X-ray diffraction data were collected at the Institut Pasteur de Montevideo (Protein Crystallography Facility) at 108 K (Cryostream Series 700; Oxford Cryosystems, Long Hanborough, UK) with a MicroMax 007-HF Cu rotating anode (Rigaku Corp., Tokyo, Japan), Varimax-HF mirrors (Rigaku Corp.) and a Mar345 image plate detector (Marresearch GmbH, Norderstedt, Germany). Data sets were processed using XDS [36] and SCALA [37]. The structure was solved by molecular replacement with AMORE [38] using the atomic coordinates of FabF from *S. aureus* (2GQD) as a search probe. Model rebuilding was performed with COOT [39], and iterative refinement with PHENIX [40] or BUSTER [41]. Re-refinement of published models was carried out with REFMAC5 [29].

Structural analysis

To evaluate conformational changes as a consequence of the I108F substitution, as well as detailed superpositions between the noncovalent and covalent cerulenin complexes, we used error-scaled difference distance matrices [25]. All comparisons were conducted with a 2 SD cut-off level to consider significant changes. The Cα values of the statistically invariant residues were used for least-squares superpositions. Simulated annealing omit maps were calculated with PHENIX [40] using the model of wtFabF in a covalent complex, without the modeled cerulenin. Model visualization and preparation of figures were performed using PYMOL [42].

Enzymatic assays: substrate preparation

The C6:0 and C10: acyl-ACPs were synthesized with AAS and *E. coli* holo-ACP, a gift from Dr John Cronan, University of Illinois, Urbana-Champaign, USA. The AAS activity was assayed using 20 μM purified *E. coli* holo-ACP and 100 μM sodium [1-^{14}C]palmitate (55 $mCi{\cdot}mmol^{-1}$),

0.1 M Tris-HCl (pH 7.8), 10 mM ATP, 10 mM $MgSO_4$, 5 mM dithiothreitol, and 0.2 μg of the AAS enzyme preparation was mixed in a 50-μL reaction system and incubated at 37 °C. The reaction mixes were then loaded onto 3MM filter disks (Whatman, Maidstone, UK), which were washed and counted for radioactivity as described by Ray and Cronan [43]. The C6:0 to C10:0 acyl-ACP were synthesized and purified according to Shen *et al.* [44] using essentially the same reaction, except that nonradioactive fatty acids replaced the radioactive substrate. We used (1-^{14}C)-labeled fatty acids of very low, specific activity (0.08 mCi·mmol^{-1}) for the synthesis of all substrates to facilitate their subsequent purification. The acyl-ACP that eluted from the octyl Sepharose (Pharmacia LKB Biotechnology AB, Uppsala, Sweden) column was lyophilized and the residue was diluted with deionized water. The samples were analyzed on 20% polyacrylamide gels containing 0.5 M urea [45] and quantified as described previously [46]. Substrates were stored at −80 °C.

[3-C^{14}]malonyl-CoA was prepared by incorporating $^{14}CO_2$ from sodium bicarbonate 40 mCi·mmol^{-1} to acetyl-CoA using a crude extract of *E. coli* BL21/pMSD8 that over-expressed the four subunits of acetyl CoA carboxylase. The reaction mix (total volume of 4 mL) contained 0.1 M Tricine-KOH buffer (pH 8.0), 1 mM ATP, 2.5 mM $MgCl_2$, 100 mM KCl, 1 mM $NaH^{14}CO_2$ (40 μCi), 1 mM dithiothreitol, 0.5 mM acetyl-CoA, and up to 2 mg of cell-free extract protein pretreated with cerulenin. The reaction was incubated for 2 h at 37 °C and stopped with 10% trichloroacetic acid. The product was purified with C18 SepPak columns. Briefly, the trichloroacetic acid supernatant was loaded into pre-equilibrated columns with 10 mL of 1 mM HCl acid, washed with 10 mL of 1 mM HCl acid and then the malonyl-CoA was eluted with a 95 : 5 mix of 0.1 M ammonium acetate buffer (pH 6.5) : acetonitrile; a second purification step used the same column and the product was eluted with a mix of 5 : 95 ammonium acetate buffer: ethanol (J. Cronan, personal communication).

Decarboxylase assays

These assays measure the ability of KAS protein to decarboxylate the donor substrate [3-^{14}C]malonyl-ACP in the condensing reaction or in the elongation reaction with hexanoyl-ACP or decanoyl-ACP, forming octanoyl and dodecanoyl-ACP, respectively. The reaction mix contained: ACP 25 μM; dithiothreitol, 1 mM; Tris-HCl, buffer 0.1 M (pH 7.5) and 3 mM, β-mercaptoethanol. [3-^{14}C]malonyl-CoA was generated *in situ* from ACP and [3-^{14}C] malonyl-ACP (26500 d.p.m.·μL^{-1}, 24 mCi·mmol^{-1}) using 1 μg of FabD in 25 mM potassium phosphate buffer (pH 6.8) in a 25-μL final volume. The reaction was incubated for 2 min before other components were added. The reaction mix was incubated at 37 °C in eppendorf tubes with a filter disk inside the caps impregnated with $BaCl_2$ to trap the CO_2 released from the reaction. The reaction was stopped opening the tubes and the radioactivity in the filter disk was counted.

Ketoacyl-ACP synthase assay

The KAS activities for *Ec*FabF and *Ec*FabFI108 were assayed according to Garwin *et al.* [26]. Briefly, the assays contained hexanoyl- or octanoyl-ACP between 0 and 100 μM, 50 μM [2-^{14}C]malonyl-CoA (specific activity, 52 Ci·mol^{-1}), 100 μM ACP, 1 μg of *Ec*FabD and the indicated amount of *Ec*FabF or *Ec*FabFI108 in a final volume of 20 μL. To ensure the linearity of the assay, we carried out the enzyme activity assays with a range of substrate concentrations, protein concentrations and incubation times (results not shown). ACP was reduced by 0.3 mM dithiothreitol before the other reaction components were added. After incubation of the sample at 37 °C for 20 min, the reaction was stopped by adding 0.4 mL of freshly prepared reducing agent containing 0.1 M K_2HPO_4, 0.4 M KCl, 30% tetrahydrofuran, and 5 mg·mL^{-1} $NaBH_4$. The reaction mixtures were vigorously agitated and incubated at 37 °C for 40 min, followed by extraction with 0.4 mL of toluene. To address the effect of cerulenin on KAS activity, 1 ng of either the FabB or FabF protein was incubated at room temperature with 0, 5, 10, 50, 100 or 200 μM cerulenin for 7 min before initiation of the condensation reaction. A final volume of 25 μL contained 200 mM potassium phosphate buffer (pH 7.8), 0.6 mM β-mercaptoethanol, 1 mM EDTA, 50 μM ACP, 200 mM malonyl-CoA, 0.6 mU MTA and 30 μM C12:0-ACP.

In vitro FAS assay

Cell-free extracts used to assay FAS activity were obtained from cultures of strains GS76 and JH642, grown in LB medium and harvested at mid exponential phase. The reaction mixture contained 0.1 M sodium phosphate (pH 7), 5 mM β-mercaptoethanol, 3 mM EDTA, 5 mM dithiothreitol, 0.7 mM NADP, 9 mM glucose 6-phosphate, 0.1 units of Glc6P DH, 20 μM ACP, 20 μM isovaleryl-CoA, 40 μM malonyl-CoA, 4 μM [2-^{14}C]malonyl-CoA and 50 μg of the 40–70% ammonium sulfate fraction of protein extracts, in a final volume of 50 μL. Cerulenin, when present, was added to a final concentration of 10 μg·mL^{-1} to protein extracts and preincubated for 10 min at 37 °C, and the reaction was started by addition of the remaining components. After incubation at 37 °C for 20 min, the reaction was stopped by addition of 10% w/v KOH. Free fatty acids were extracted with hexane and quantified in a scintillation counter.

β-Galactosidase-specific activity

β-Galactosidase-specific activity (ΔD_{420} min^{-1}·mL^{-1}·$culture^{-1}$ × $1000/D_{525}$) was determined as described previously [47] after pelleting cell debris.

Acknowledgements

This present study was supported by grants received from the Consejo Nacional de Investigaciones Científicas y Técnicas (CONICET) and Agencia Nacional de Promoción Científica y Tecnológica (FONCYT). FF is a fellow from CONICET, and SA, DdeM and GES are career investigators from CONICET. We acknowledge institutional support from the Institut Pasteur de Montevideo, and access to its Protein Crystallography Facility. FT is a research scientist and NL staff technician from the Institut Pasteur de Montevideo. AB is a research scientist from Institut Pasteur.

Author contributions

FT, SGA, NL and FAF planned and performed experiments and analyzed data. DdM analyzed data and wrote the paper. FT, AB and GES planned experiments, analyzed data and wrote the paper.

References

1 Maier T, Jenni S & Ban N (2006) Architecture of mammalian fatty acid synthase at 4.5 A resolution. *Science* **311**, 1258–1262.
2 White SW, Zheng J, Zhang YM & Rock CO (2005) The structural biology of type II fatty acid biosynthesis. *Annu Rev Biochem* **74**, 791–831.
3 Choi KH, Heath RJ & Rock CO (2000) beta-ketoacyl-acyl carrier protein synthase III (FabH) is a determining factor in branched-chain fatty acid biosynthesis. *J Bacteriol* **182**, 365–370.
4 Schujman GE, Choi KH, Altabe S, Rock CO & de Mendoza D (2001) Response of *Bacillus subtilis* to cerulenin and acquisition of resistance. *J Bacteriol* **183**, 3032–3040.
5 de Mendoza D, Schujman GE & Aguilar PS (2002) Biosynthesis and function of membrane lipids. In Bacillus subtilis and its closest relatives: from genes to cells (Sonenshein AL, Hoch JA & Losick R, eds), pp. 43–55. ASM Press, Washington, DC.
6 Wu M, Singh SB, Wang J, Chung CC, Salituro G, Karanam BV, Lee SH, Powles M, Ellsworth KP, Lassman ME *et al.* (2011) Antidiabetic and antisteatotic effects of the selective fatty acid synthase (FAS) inhibitor platensimycin in mouse models of diabetes. *Proc Natl Acad Sci USA* **108**, 5378–5383.
7 Mashima T, Seimiya H & Tsuruo T (2009) *De novo* fatty-acid synthesis and related pathways as molecular targets for cancer therapy. *Br J Cancer* **100**, 1369–1372.
8 Parsons JB & Rock CO (2011) Is bacterial fatty acid synthesis a valid target for antibacterial drug discovery? *Curr Opin Microbiol* **14**, 544–549.
9 Noto T, Miyakawa S, Oishi H, Endo H & Okazaki H (1982) Thiolactomycin, a new antibiotic. III. *In vitro* antibacterial activity. *J Antibiot (Tokyo)* **35**, 401–410.
10 Wang J, Soisson SM, Young K, Shoop W, Kodali S, Galgoci A, Painter R, Parthasarathy G, Tang YS, Cummings R *et al.* (2006) Platensimycin is a selective FabF inhibitor with potent antibiotic properties. *Nature* **441**, 358–361.
11 Wang J, Kodali S, Lee SH, Galgoci A, Painter R, Dorso K, Racine F, Motyl M, Hernandez L, Tinney E *et al.* (2007) Discovery of platencin, a dual FabF and FabH inhibitor with *in vivo* antibiotic properties. *Proc Natl Acad Sci USA* **104**, 7612–7616.
12 Kauppinen S, Siggaard-Andersen M & Wettstein-Knowles P (1988) beta-Ketoacyl-ACP synthase I of *Escherichia coli*: nucleotide sequence of the fabB gene and identification of the cerulenin binding residue. *Carlsberg Res Commun* **53**, 357–370.
13 Price AC, Choi KH, Heath RJ, Li Z, White SW & Rock CO (2001) Inhibition of beta-ketoacyl-acyl carrier protein synthases by thiolactomycin and cerulenin. Structure and mechanism. *J Biol Chem* **276**, 6551–6559.
14 Moche M, Schneider G, Edwards P, Dehesh K & Lindqvist Y (1999) Structure of the complex between the antibiotic cerulenin and its target, beta-ketoacyl-acyl carrier protein synthase. *J Biol Chem* **274**, 6031–6034.
15 Val D, Banu G, Seshadri K, Lindqvist Y & Dehesh K (2000) Re-engineering ketoacyl synthase specificity. *Structure* **8**, 565–566.
16 Schujman GE, Altabe S & de Mendoza D (2008) A malonyl-CoA-dependent switch in the bacterial response to a dysfunction of lipid metabolism. *Mol Microbiol* **68**, 987–996.
17 Joosten RP, Salzemann J, Bloch V, Stockinger H, Berglund AC, Blanchet C, Bongcam-Rudloff E, Combet C, Da Costa AL, Deleage G *et al.* (2009) PDB_REDO: automated re-refinement of X-ray structure models in the PDB. *J Appl Crystallogr* **42**, 376–384.
18 Huang W, Jia J, Edwards P, Dehesh K, Schneider G & Lindqvist Y (1998) Crystal structure of beta-ketoacyl-acyl carrier protein synthase II from *E. coli* reveals the molecular architecture of condensing enzymes. *EMBO J* **17**, 1183–1191.
19 Olsen JG, Kadziola A, Wettstein-Knowles P, Siggaard-Andersen M, Lindquist Y & Larsen S (1999) The X-ray crystal structure of beta-ketoacyl [acyl carrier protein] synthase I. *FEBS Lett* **460**, 46–52.

20 Price AC, Rock CO & White SW (2003) The 1.3-Angstrom-resolution crystal structure of beta-ketoacyl-acyl carrier protein synthase II from *Streptococcus pneumoniae*. *J Bacteriol* **185**, 4136–4143.
21 Campobasso N, Patel M, Wilding IE, Kallender H, Rosenberg M & Gwynn MN (2004) *Staphylococcus aureus* 3-hydroxy-3-methylglutaryl-CoA synthase: crystal structure and mechanism. *J Biol Chem* **279**, 44883–44888.
22 Mathieu M, Zeelen JP, Pauptit RA, Erdmann R, Kunau WH & Wierenga RK (1994) The 2.8 A crystal structure of peroxisomal 3-ketoacyl-CoA thiolase of *Saccharomyces cerevisiae*: a five-layered alpha beta alpha beta alpha structure constructed from two core domains of identical topology. *Structure* **2**, 797–808.
23 Funabashi H, Kawaguchi A, Tomoda H, Omura S, Okuda S & Iwasaki S (1989) Binding site of cerulenin in fatty acid synthetase. *J Biochem* **105**, 751–755.
24 Funabashi H, Iwasaki S, Okuda S & Omura S (1983) A model study on the mechanism of fatty acid synthetase inhibition by antibiotic cerulenin. *Tetrahedron Lett* **24**, 2673–2676.
25 Schneider TR (2000) Objective comparison of protein structures: error-scaled difference distance matrices. *Acta Crystallogr D Biol Crystallogr* **56**, 714–721.
26 Garwin JL, Klages AL & Cronan JE Jr (1980) Structural, enzymatic, and genetic studies of beta-ketoacyl-acyl carrier protein synthases I and II of *Escherichia coli*. *J Biol Chem* **255**, 11949–11956.
27 Counterman AE & Clemmer DE (1999) Volumes of individual amino acid residues in gas-phase peptide ions. *J Am Chem Soc* **121**, 4031–4039.
28 Wimley WC & White SH (1996) Experimentally determined hydrophobicity scale for proteins at membrane interfaces. *Nat Struct Biol* **3**, 842–848.
29 Murshudov GN, Skubak P, Lebedev AA, Pannu NS, Steiner RA, Nicholls RA, Winn MD, Long F & Vagin AA (2011) REFMAC5 for the refinement of macromolecular crystal structures. *Acta Crystallogr D Biol Crystallogr* **67**, 355–367.
30 Heath RJ & Rock CO (1996) Inhibition of beta-ketoacyl-acyl carrier protein synthase III (FabH) by acyl-acyl carrier protein in *Escherichia coli*. *J Biol Chem* **271**, 10996–11000.
31 Edwards P, Nelsen JS, Metz JG & Dehesh K (1997) Cloning of the fabF gene in an expression vector and *in vitro* characterization of recombinant fabF and fabB encoded enzymes from *Escherichia coli*. *FEBS Lett* **402**, 62–66.
32 Albanesi D, Reh G, Guerin ME, Schaeffer F, Debarbouille M, Buschiazzo A, Schujman GE, de Mendoza D & Alzari PM (2013) Structural basis for feed-forward transcriptional regulation of membrane lipid homeostasis in *Staphylococcus aureus*. *PLoS Pathog* **9**, e1003108.
33 de Mendoza D, Klages UA & Cronan JE Jr (1983) Thermal regulation of membrane fluidity in *Escherichia coli*. Effects of overproduction of beta-ketoacyl-acyl carrier protein synthase I. *J Biol Chem* **258**, 2098–2101.
34 Vagner V, Dervyn E & Ehrlich SD (1998) A vector for systematic gene inactivation in *Bacillus subtilis*. *Microbiology* **144** (Pt 11), 3097–3104.
35 Jiang Y, Chan CH & Cronan JE (2006) The soluble acyl-acyl carrier protein synthetase of *Vibrio harveyi* B392 is a member of the medium chain acyl-CoA synthetase family. *Biochemistry* **45**, 10008–10019.
36 Kabsch W (2010) XDS. *Acta Crystallogr D Biol Crystallogr* **66**, 125–132.
37 Evans PR (2011) An introduction to data reduction: space-group determination, scaling and intensity statistics. *Acta Crystallogr D Biol Crystallogr* **67**, 282–292.
38 Trapani S & Navaza J (2008) AMoRe: classical and modern. *Acta Crystallogr D Biol Crystallogr* **64**, 11–16.
39 Emsley P & Cowtan K (2004) Coot: model-building tools for molecular graphics. *Acta Crystallogr D Biol Crystallogr* **60**, 2126–2132.
40 Afonine PV, Grosse-Kunstleve RW, Echols N, Headd JJ, Moriarty NW, Mustyakimov M, Terwilliger TC, Urzhumtsev A, Zwart PH & Adams PD (2012) Towards automated crystallographic structure refinement with phenix.refine. *Acta Crystallogr D Biol Crystallogr* **68**, 352–367.
41 Bricogne G, Blanc E, Brandl M, Flensburg C, Keller P, Paciorek W, Roversi P, Sharff A, Smart OS & Vonrhein C (2011) BUSTER. [2.8.0]. Global Phasing Ltd., Cambridge, UK, Ref Type: Computer Program.
42 DeLano WL (2002) The PyMOL Molecular Graphics System. DeLano Scientific, San Carlos, CA, USA, Ref Type: Computer Program.
43 Ray TK & Cronan JE Jr (1976) Activation of long chain fatty acids with acyl carrier protein: demonstration of a new enzyme, acyl-acyl carrier protein synthetase, in *Escherichia coli*. *Proc Natl Acad Sci USA* **73**, 4374–4378.
44 Shen Z, Fice D & Byers DM (1992) Preparation of fatty-acylated derivatives of acyl carrier protein using *Vibrio harveyi* acyl-ACP synthetase. *Anal Biochem* **204**, 34–39.
45 Post-Beittenmiller D, Jaworski JG & Ohlrogge JB (1991) *In vivo* pools of free and acylated acyl carrier proteins in spinach. Evidence for sites of regulation of fatty acid biosynthesis. *J Biol Chem* **266**, 1858–1865.
46 Rock CO, Garwin JL & Cronan JE Jr (1981) Preparative enzymatic synthesis of acyl-acyl carrier protein. *Methods Enzymol* **72**, 397–403.

47 Miller JH (1972) Experiments in Molecular Genetics. Cold Spring Harbor Laboratory, Cold Spring Harbor, NY.
48 Schujman GE, Grau R, Gramajo HC, Ornella L & de Mendoza D (1998) *De novo* fatty acid synthesis is required for establishment of cell type-specific gene transcription during sporulation in *Bacillus subtilis*. *Mol Microbiol* **29**, 1215–1224.
49 Cronan JE (2006) A family of arabinose-inducible *Escherichia coli* expression vectors having pBR322 copy control. *Plasmid* **55**, 152–157.
50 Davis MS, Solbiati J & Cronan JE Jr (2000) Overproduction of acetyl-CoA carboxylase activity increases the rate of fatty acid biosynthesis in *Escherichia coli*. *J Biol Chem* **275**, 28593–28598.